

# Robust Design Optimization of Coaxial Rotor for UAV Application Considering Operational Uncertainty

Sangook Jun<sup>\*</sup>, Kwanjung Yee<sup>\*\*</sup>, Jaewon Lee<sup>\*\*</sup>, Dong-ho Lee<sup>†</sup>

<sup>\*</sup> School of Mechanical and Aerospace Engineering, Seoul National University,  
Seoul, 151-742, Republic of Korea

<sup>\*\*</sup> Department of Aerospace Engineering, Pusan National University,  
Busan, 609-735, Republic of Korea

<sup>†</sup> Institute of Advanced Aerospace Technology, SNU IAAT,  
School of Mechanical and Aerospace Engineering, Seoul National University  
Seoul, 151-742, Republic of Korea

## ABSTRACT

This research aims at performing robust design optimization by taking into account operational uncertainties to improve the performance of the coaxial rotor unmanned aerial vehicle (UAV) that is under development. For this sake, neural network models are constructed for aerodynamic performance obtained from a source-doublet panel method coupled with a time-marching free wake method. Two kinds of operational uncertainties are considered such as ballistic damage on blades and weight variation due to the mission change. Approximate moment approach is employed to evaluate the robustness of performance. Subsequently, a relationship between the robustness of performance indices and the parameters representing blade geometry is investigated. In addition, we study the robustness of the performance indices and constraints for three different solutions chosen from the Pareto optima set. It is confirmed that the trend of design variables to improve performance is in contradiction to the robustness of design. Besides, by incorporating the robust design method, a probability for a designed coaxial rotor to accomplish missions successfully can be improved from about 50% to 70%~95% under the uncertainty such as ballistic damage.

## Nomenclature

$AI$	: autorotation index
$C_d, C_D$	: drag coefficient
$C_{d,damage}$	: $C_d$ of the damaged airfoil
$C_l, C_L$	: lift coefficient
$C_{l\alpha}$	: $C_l$ at angle of attack zero
$C_{l\alpha,damage}$	: $C_{l\alpha}$ of the damaged airfoil
$C_P$	: total power coefficient
$C_T$	: thrust coefficient
$D$	: rotor diameter
$f$	: objective function
$\bar{f}$	: averaging objective function
$FM$	: figure of merit
$g_i$	: $i$ -th constraint
$\bar{g}$	: averaging constraint
$GW$	: gross weight
$k$	: sigma level
$\mathbf{p}$	: system parameter vector
$P_{available}$	: available power
$R_U/R_L$	: differential rotor radii
$V_{climb}$	: vertical climb rate
$W_{blade}$	: weight of blades
$\mathbf{x}$	: design variable vector
$\mathbf{x}^L$	: lower bound of design variables
$\mathbf{x}^U$	: upper bound of design variables

$\theta$	: pitch angle of blade elements
$\theta_{75}$	: collective pitch angle
$\theta_{tw}$	: twist angle
$\lambda$	: induced power factor
$\lambda_{in}$	: inflow rate
$s$	: deviation or solidity
$w$	: weights

## Introduction

Increases in crime and budget pressure are forcing the military to seek technologies that allow for a more effective performance of their missions. The concept of having a small and maneuverable UAV that can be operated in the field to perform sky surveillance, remote sensing, and communication relay is very appealing.

A coaxial rotor configuration can be a viable UAV platform because it provides significant advantages over fixed-wing vehicles by the capabilities of hovering and loitering. Moreover, the coaxial rotor configuration enables a more compact design than the conventional helicopter configuration so that it can be carried by a single person. The small size of the platform

also means that it is light weight, thus allowing for easy handling in the field.[1]

Mainly inspired by the superior lifting capability and advantages of compact size, Pusan National University started developing a prototype of a small multi-purpose UAV.[2] After a series of trade-off study in the year 2005, the coaxial rotor system is chosen for the basic platform for the UAV research.

The coaxial rotor UAV is anticipated to operate in a critical and hazardous environment like in a battle field. As a result, due to unexpected accidents (operational uncertainty), the rotor performance may be most likely be degraded. The ballistic vulnerability is an important consideration for military helicopters including the coaxial rotor UAV because they generally fly at a lower altitude and slower speed than the fixed-wing aircraft. Therefore, in order to minimize unexpected attrition of helicopter forces, any performance degradation must be minimized and, if possible, be prevented to ensure a continued success on the battlefield.[3] Since the rotor of helicopters itself provides all forces including lift, propulsion, and control, any damage inflicted to the main rotor systems is more likely to cause serious consequences. In addition, the coaxial rotor UAV is employed in various missions such as reconnaissance, border surveillance, delivery of non-lethal agents, search and rescue support, and chemical/biological agent detection. This means that the UAV carries payloads of diverse types in accordance to the specified flight mission. In certain cases, the payload may exceed the designed total gross weight to enable the mission accomplishment. Since the failure during the given mission may result in the loss of human lives and the valuable vehicle, uncertainty associated with the mission operation is an essential factor to be considered in the design of a coaxial rotor UAV. Consequently, the analysis of robust design optimization is imperative, in the sense that it minimizes the performance degradation by taking into account the operational uncertainty as design requirements.

The robust design optimization is a design method of which the objective is to minimize the deviation of a target performance with respect to an external variation (uncertainty). In a mathematical/statistical sense, one assures robustness by decreasing the size of performance deviation and thus minimizing the performance degradation. The history of this robust design optimization ascends to the late 80s', when Taguchi [4] proposed a methodology

of determining design variables that are insensitive to noises in the manufacturing process. His research became the foundation for the robust design, which is followed by intensive researches on the robust design optimization [5-9]. DeLaurentis and Mavris [5] perform a robust design of a high-speed civil transport based on the uncertainty modeling and the formal method for management of uncertainty. Jun et al [9] utilizes a neural network model in conjunction with Monte-Carlo simulations for the robust design of the wing of an aircraft under the operational and manufacturing uncertainty. In light of the remarkable evolution of the robust design optimization, it is meaningful to apply the robust design method to real problems involving actual systems such as a coaxial rotor UAV.

The objective of this research is to design a coaxial rotor UAV that has minimum performance degradation by taking into account the operational uncertainty. To this end, an uncertainty model is built for the ballistic damage and the weight variation due to the mission change. Then an optimization problem is formulated for multiple objectives incorporating different weight parameters between the performance and its variation. In addition, in order to ensure the robustness of constraints, we add a multiplicative term consisting of the constraints deviation and a sigma level into the constraints. As a consequence, the result of the robust design optimization is compared with that of general design optimization to discuss the importance and the limitation of the robust design optimization. Next, Pareto optimum sets with respect to the sigma level are proposed, and then a relationship between the performance and the robustness is investigated from the tendency of design variables towards robustness. Finally, the performance distribution over the given design region is discussed by observing the Pareto set whenever the sigma level of the constraints increases.

## Design Problem Formulation

### *Robust design optimization*

The robust design optimization (RDO) is given as follows:

$$\begin{aligned} & \text{minimize } \bar{f}(\mathbf{x}, \mathbf{p}) + \mathbf{s}_f \\ & \text{subject to } \bar{g}_i(\mathbf{x}, \mathbf{p}) + k\mathbf{s}_g \leq 0 \quad i = 1, \dots, m \quad (1) \\ & \mathbf{x}^L \leq \mathbf{x} \leq \mathbf{x}^U \end{aligned}$$

Where,  $\mathbf{x}$  is the design variable vector,  $\mathbf{p}$  is the system parameter vector, and  $m$  is the number of constraints. In Eq. (1),  $\mathbf{x}^L$  denotes the lower bound of design variables and  $\mathbf{x}^U$  denotes the upper bound.  $\bar{f}$  and  $\bar{g}$  are average values of the objective function and the constraints, respectively.  $s$  is deviation of the objective function and the constraints. The sigma level in conjunction with  $k$  in the constraints expression is an index that indicates the probability of satisfying the given constraint.

The uncertainty model of the design variables and parameters should be constructed in order to assess the objective function and constraints in Eq. (1). However, it is nearly impossible to construct the uncertainty model because one lacks the information about when and how the uncertainty will occur. Subsequently, it is reasonable to assume that all uncertainties under consideration follow the normal distribution according to a statement: “*various natural phenomena follow the Gaussian distribution*” [10]. The approximate moment approach (AMA) [8], in conjunction with this assumption, is employed to obtain the mean and the deviation of objective function and constraints.

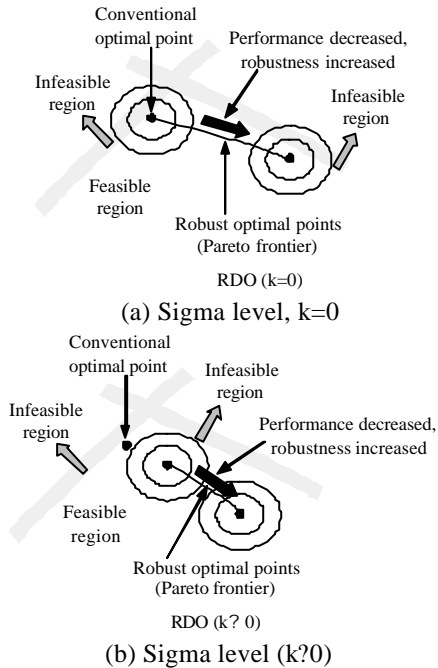


Fig. 1. Schematics of Pareto optima in robust design optimization

If one considers the robustness of an objective function, as shown in Fig. 1(a), the Pareto optima may violate the constraints. However, if the sigma level of constraints has specific values determined by a design

requirement or a designer, the confidence interval is completely contained in the safe region as shown in Fig. 1(b).

#### Baseline configuration

Figure 2 shows a coaxial UAV prototype developed by the Pusan National University, which is based on a series of trade-off studies and statistical data. This coaxial UAV is adopted for a baseline configuration for the design optimization given in the following. An electric motor with batteries against an internal engine with fuel is selected for the drive system, which ensures low noise, small vibration, and little detectability.



Fig. 2. Configuration of the coaxial rotor UAV designed by the Pusan National University

Table 1. Baseline configuration & performance of the coaxial rotor UAV

Coaxial rotor geometry	
Rotor diameter (D)	1572 mm
Differential rotor radii ( $R_U/R_L$ )	1.0
Anhedral angle	0.0°
Twist	0.0°
Taper	1.0
Vertical separation (H/D)	0.120
Airfoil	VR13
Solidity ( $s$ )	0.0955
Performance	
$C_T/s$	0.0578
$C_P/s$	0.0058
Figure of Merit (FM)	0.5306
Gross Weight (GW)	14.0 kg
Thrust (T)	137.34 N
Autorotation index (AI)	9.2863
Weight of blade ( $W_{blade}$ )	0.5520 kg
Vertical climb rate ( $V_{climb}$ )	87.37 m/min
Available power ( $P_{available}$ )	200.0 W

The rotor geometry and the flight performance of the baseline coaxial rotor are summarized in Table 1. The term vertical separation means that the upper rotor is separated from the lower one by a distance of

0.12D. The rotor performance in Table 1 is calculated taking the take-off gross weight of 14 kg into consideration. The thrust required for hovering is 137.34N and the figure of merit is about 0.53, which is a little lower as compared to a full-scale conventional helicopter.

#### *Aerodynamic analysis*

For the design purpose of a coaxial rotor, an efficient aerodynamic analysis tool that provides a faithful outcome like the panel method is necessary. Therefore, the source-doublet panel method developed by Lee et al is utilized. In this tool, time-marching free wake model is implemented and the diffusion of vortex filament core is considered for the stability of the rotor wake. Rigorous aerodynamic analysis and the validation can be found in the reference by Lee et al [12].

Tip wake geometry in hover and steady forward flight is shown in Fig. 3, in which wake are continuously generated to simulate the temporal evolution of the rotor wake.

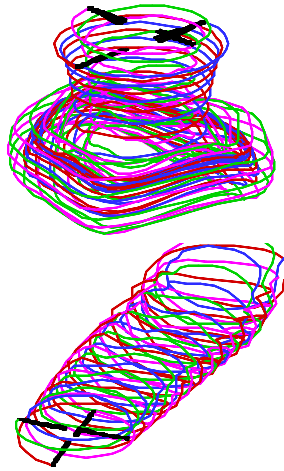


Fig. 3. Hover and steady forward flight results of a source-doublet panel method with a time-marching free wake model

#### *Design variables*

Based on parametric studies by Lee et al[12], the rotor diameter, the differential rotor radii ( $R_U/R_L$ ), the taper, and the twist angle are opted for design variables, of which the upper and lower bounds are chosen according to the ranges in Table 2. Furthermore, the VR13 airfoil is chosen for this research since it shows superior aerodynamic performance over any other airfoils.

Table 2. Ranges of design variables

Design parameters	Lower bound	Upper bound
Rotor diameter (D=1572 mm)	0.9D	1.1D
Differential rotor radii ( $R_U/R_L$ )	0.8	1.0
Twist (degree)	-14°	-8°
Taper	1	3

#### *Definition of the uncertainty model*

For the RDO in this study, we construct two uncertainty models in terms of design variables and parameters, namely the operational uncertainty and the manufacturing uncertainty. The operational uncertainty contains ballistic damage of airfoil, deformation of airfoil due to dust, payload change, and varying maximum operational range or endurance time. In this study we are unable to directly incorporate the maximum operational range of the endurance time because of the use of hover performance. Nonetheless, we take these uncertainties into consideration in the manner that the extension of range or endurance time is indirectly related to the weight increase due to the extra battery packs required for the extended operation. In addition, we model the degradation of the rotor performance caused by ballistic damage, dust, or icing, as the reduced lift and drag coefficients as well as the area decrease due to the damaged blade. Furthermore, the manufacturing tolerance is modeled as an uncertainty, albeit it has little effect on the coaxial rotor UAV operation.

#### *Damaged blade area*

The variations of  $C_l$ ,  $C_d$  resulting from the damage or deformation of an airfoil are correlated with each other, which implies that it is unlikely to get constant  $C_d$  with decreasing  $C_l$ . As a matter of fact, finding the relationship between these two variables is difficult, thus we determine the values of  $C_l$ , and  $C_d$  whose values are rendered maximum by utilizing the results obtained from different research. Then we always incorporate the fixed values of  $C_l$ , and  $C_d$  to estimate the performance of the rotor blade. With an extra parameter of the area change due to the damaged or deformed blade, we construct an uncertainty model which deals with the performance degradation of the airfoil due to the ballistic damage, dust, or icing.

In accordance with the experimental study on a ballistic damage of the SC1095-R8 Airfoil by Leishman [3,13], a hole close to the leading

edge is known to cause the maximum reduction of the aerodynamic performance (40% decrease in  $C_L$ , 300% increase in  $C_d$ ) when the airfoil is subject to the stall angle of attack of 15 degrees. The Boeing 737-200 wing model dealing with the effects of ice on lift and drag [14] shows that 30% decrease of  $C_L$  and 200% increase of  $C_D$  at the stall angle of attack. The NLF0414 airfoil appears to have 30%~40% reduction of  $C_L$  due to the effect of the ice over of the stall region [15]. Because the information about the VR13 airfoil in damaged conditions lacks in the literature, we prefer to adopt the results from Leishman (40% decrease in  $C_L$ , 300% increase in  $C_d$ ), albeit being obtained for different airfoil as compared to the VR13. Subsequently, the performance degradation related to the thrust and the required power due to airfoil damages is formulated as a function with respect to the blade area.

Assume a blade tip which is critical for the ballistic damage effect is damaged. It follows that the thrust coefficient ( $C_T$ ) can be given in Eq. (2)

$$C_T = \frac{1}{2} s C_{la} \int_0^d [\lambda(r) r^2 - \lambda(r) r] dr + \frac{1}{2} s C_{la,damage} \int_d^1 [\lambda(r) r^2 - \lambda(r) r] dr \quad (2)$$

where,  $C_{la,damage} = 0.6 C_{la}$

where the integration interval is chosen as  $[0, 1]$  which ranges from the root to the tip radius, and  $d$  is the starting location of the damage chosen from  $0 = d = 1$ . In addition, the second term  $C_{la,damage}$  in the right hand side is the  $C_{la}$  of the damaged airfoil, which is reduced by 40% from the nominal one by taking into account the 40% reduction of  $C_L$ .

Because we assume linearly twisted blades in this study, the pitch angle at the blade element  $\lambda(r)$  can be calculated by using the reference blade-pitch angle (collective pitch,  $\lambda_{75}$ ) at the 3/4-radius and the blade twist rate per radius of the rotor ( $\lambda_{tw}$ ). In addition, at the hovering condition, the inflow rate  $\lambda(r)$  can be expressed in a simple form in Eq. (3).

$$\lambda(r) = \lambda_{75} + (r - 0.75) \lambda_{tw} \quad (3)$$

$$\lambda(r) = \frac{s C_{la}}{16} \left( \sqrt{1 + \frac{32}{s C_{la}} \lambda(r) r} - 1 \right)$$

From Eqs. (2) and (3), it follows that the  $C_T$  is a function of collective pitch angle and damaged area, as shown in Fig. 4.

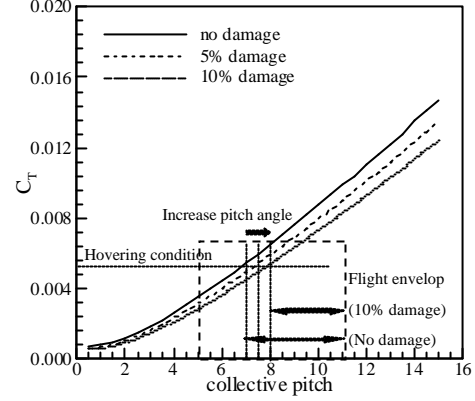


Fig. 4. Variation in rotor thrust coefficient with collective pitch for rotors with different damaged area

Fig. 4 shows that the  $C_T$  is reduced by 9.7% and 17.4% corresponding to 5% damage and 10% damage over no damage at the same collective pitch, respectively. Also, in order to maintain the hover condition, the collective pitch should be increased, which has an effect on reduced stall margin and therefore a smaller flight envelop.

On the other hand, the total power coefficient ( $C_P$ ) is expressed by a sum of the induced power (the first and second terms on the right hand side) and the profile power (the third and fourth terms on the right hand side), as given in Eq. (4). Note that  $C_{d,damage}$  represents the  $C_d$  of the damaged airfoil, which is 300% greater than nominal one.

$$C_P = \int_{r=0}^{r=d} \lambda(r) dC_T + \left[ \int_{r=d}^{r=1} \lambda(r) dC_T \right]_{damage} + \frac{1}{2} \int_0^d s C_d r^3 dr + \frac{1}{2} \int_d^1 s C_{d,damage} r^3 dr, \quad (4)$$

where,  $C_{d,damage} = 3 C_d$

Finally, along the definition of figure of merit ( $FM$ ) in Eq. (5), it can be obtained by using Eqs. (2) and (4) as follows:

$$FM = \frac{\text{ideal power}}{\text{induced power} + \text{profile power}} \quad (5)$$

$$= \frac{P_{ideal}}{k P_{ideal} + P_0}$$

where  $k$  represents the induced power factor. We adopt  $k = 1.2$  since we deal with a coaxial rotor UAV as opposed to a conventional helicopter, which has been determined via a graph fitting method using the  $FM$  obtained from the approximate model.

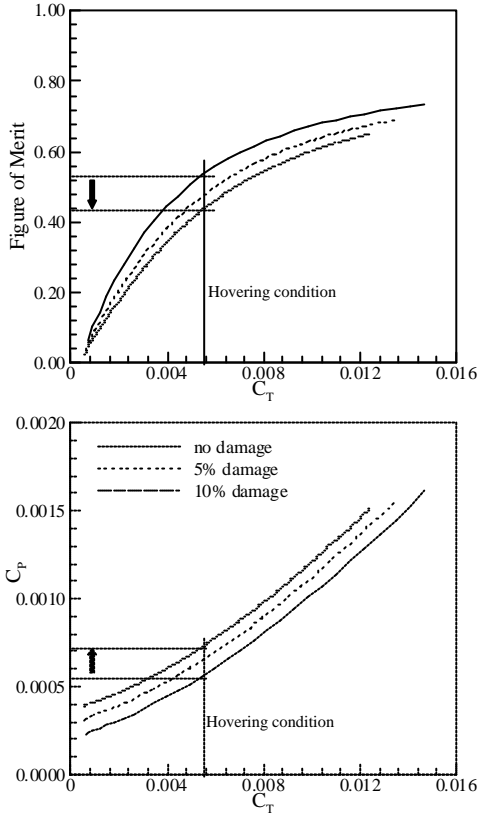


Fig. 5. Hover performance degradation due to ballistic damage on blade

Fig. 5 illustrates the hover performance via Eqs. (5) and (6), which shows that attaining the same thrust at 10% damage requires 30% increase in the  $C_p$ , and the  $FM$  decreases by 17% from no damage condition.

The uncertainty model discussed so far is constructed for the case of ballistic damage in the battlefield, however, it can possibly be adopted to deal with the rotor performance variation due to icing or dust by incorporating the blade area change.

### Mission change

In order to accomplish various missions such as reconnaissance and rescue support, various different types of payload should be considered. For instance, it might be the case that an additional battery pack is needed to improve the endurance time or the operational range, as mentioned earlier. The take-off gross weight is chosen by 14 kg, however, a multi-role coaxial rotor UAV should be designed such that it has the operational performance in spite of the overweight. Hence, we construct an uncertainty model which deals with not only the payload variation due to mission change but also the

total weight change of the system.

### Tolerance

The tolerance uncertainty, albeit nonfatal to the UAV operation, is an uncertainty which often occurs in the manufacturing process. Even though a complete elimination of the tolerance uncertainty seems to be unattainable, most of this uncertainty effect can probably be removed by precision manufacturing at significant cost. In contrast, by taking into account the tolerance effect on the design stage one can take advantage of not only easy accessibility of fabrication, but also cost reduction. Consequently, in this study we specify the tolerance of the rotor geometry by 2% variation of the design variable ranges in Table 2. The tolerance variation is randomly chosen for the purpose of identifying a major factor affecting the operation of the coaxial rotor UAV such as the operational uncertainty.

Table 3. Uncertainty models

Uncertainty factors		Mean	Deviation
Operating uncertainty	Damaged blade area*	1.0 A	0.05 A
	weight (kg)	14.0	$5.00 \times 10^{-1}$
Manufacturing uncertainty	Rotor diameter (M)	1.572	$6.29 \times 10^{-3}$
	$R_U/R_L$	0.9	$4.00 \times 10^{-3}$
	Twist (degree)	-11.0	$1.20 \times 10^{-1}$
	Taper	2.0	$4.00 \times 10^{-2}$

$$* C_l = 0.6C_{l,VR13}, C_d = 3.0C_{d,VR13}$$

Table 3 summarizes the uncertainty models discussed so far, where the deviations of each model are determined based on the design requirements.

Here,  $A$  is the total area of four blades and the coefficients with the term VR13 represent the  $C_l$  and  $C_d$  of the VR13 airfoil. The RDO problem defined in following section is solved by employing the uncertainty model shown in Table 3.

### Problem definition

In order to minimize the performance degradation of the coaxial rotor UAV, robust design optimization has been performed for two cases. In the first case, the optimization is performed to maximize figure of merit ( $FM$ ) of

the coaxial rotor. On the other hand, the available power ( $P_{available}$ ) is maximized in the second case, which dictates that the vertical climb and the maneuver in forward flight are enabled. The objective functions for each case are formulated by the weighted sum of both the performance and its deviation.

Case 1: Maximize *Figure of Merit* in hover

$$\text{Max. } \mathbf{w} \cdot FM - (1 - \mathbf{w}) \cdot \mathbf{s}(FM)$$

$$\text{s.t. } Thrust = GW$$

$$\begin{aligned} AI - k \cdot \mathbf{s}(AI) &\geq AI_{baseline} \\ W_{blade} + k \cdot \mathbf{s}(W_{blade}) &\leq 1.3(W_{blade})_{baseline} \\ V_{climb} - k \cdot \mathbf{s}(V_{climb}) &\geq (V_{climb})_{baseline} \\ P_{available} - k \cdot \mathbf{s}(P_{available}) &\geq (P_{available})_{baseline} \end{aligned}$$

Case 2: Maximize *available power* for vertical climb or forward flight

$$\text{Max. } \mathbf{w} \cdot P_{available} - (1 - \mathbf{w}) \cdot \mathbf{s}(P_{available})$$

$$\text{s.t. } Thrust = GW$$

$$\begin{aligned} AI - k \cdot \mathbf{s}(AI) &\geq AI_{baseline} \\ W_{blade} + k \cdot \mathbf{s}(W_{blade}) &\leq 1.3(W_{blade})_{baseline} \\ V_{climb} - k \cdot \mathbf{s}(V_{climb}) &\geq (V_{climb})_{baseline} \\ FM - k \cdot \mathbf{s}(FM) &\geq FM_{baseline} \end{aligned}$$

where the subscript ‘baseline’ represents the baseline coaxial rotor configuration given in Table 1. The terms  $GW$  and  $AI$  denote the gross weight and the autorotation index, respectively.  $W_{blade}$ , is the weight of blade and  $V_{climb}$  is the vertical climb rate. The standard deviation of  $F$  is represented by  $\mathbf{s}(F)$ . If  $k=0$  and  $\mathbf{?}=1$ , the formulation collapses to a DO problem that simply maximizes  $FM$  or  $P_{available}$ .

Since the optimization is carried out for hovering condition in the first and second cases, the required thrust must be equal to the gross weight of the coaxial rotor UAV. In addition, the  $AI$  of the designed rotor should be greater than the baseline value in order to guarantee safe landing. The  $W_{blade}$  is one of the crucial factors that affect the aerodynamic performance and the manufacturing cost. Hence,  $W_{blade}$  is constrained to have less than 1.3 times the baseline rotor weight. In other words, the  $W_{blade}$  should not exceed 1% of the gross take off weight (14kg). Different from the first case, the second case deals with the objective function of  $P_{available}$ . Subsequently, an additional constraint condition is imposed such that  $FM$  should be greater than that of the baseline, which implies that the designed rotor generates sufficient power for hover.

The change in rotor geometry will result in a

change in weight, which in turn affects the rotor performance such as  $FM$  and  $V_{climb}$ . Hence, the change in weight due to the variation of rotor geometry is taken into account. In addition, the conditions related to  $AI$  and  $W_{blade}$  are imposed to overcome a limitation of optimization design such as structural instability.

*Construction of the artificial neural network models*

In order to perform the efficient design optimization, an artificial neural network (ANN) model[16] replaces the aerodynamic analysis. For the optimization design of the coaxial rotor blade, a total of 88 experimental points are chosen via the D-optimal experimental design. The aerodynamic analyses using the source-doublet panel method with a time-marching free wake model are performed for obtaining the  $FM$ ,  $C_T/s$ , and  $C_P/s$ . The ANN models, which are composed of an input layer with 5 neurons (four design variables and one collective pitch angle), a hidden layer with 8 neurons, and an output layer with 4 neurons, are constructed. Note that the 88 experimental data points are utilized for model learning. The coefficient of determination ( $R^2$ ) and the root mean squared error ( $RMSE$ ) are evaluated to validate the generation of alternative models, as summarized in Table 4. Of the entire approximate models, the coefficients of determination are greater than 0.99 and the  $RMSE$  are smaller than 0.02, thus ensuring reliable prediction capability of the artificial neural network models.

Table 4. Results of ANOVA (Analysis of variance)

	Solidity (s)	Figure of Merit	$C_T/s$	$C_P/s$
$R^2$	0.9997	0.9985	0.9989	0.9993
$RMSE$	0.0095	0.0200	0.0170	0.0137

## Results

In this study, a conventional design optimization (DO) is performed for a coaxial rotor configuration together with the RDO. By the DO, it represents any design method based on the deterministic concept without the concept of robustness. The hover performance function is approximated using the ANN in the design space. An optimal solution is sought by invoking a sequential quadratic programming method.

### Pareto optimal sets

Fig. 6 shows the Pareto front obtained from RDO with respect to the varying weight (?) of the objective function from 0 to 1, together with increasing sigma level ( $k$ ). The  $k$  value is chosen such that it allows performing RDO, which is up to  $k=1.5$  in case 1 and is up to  $k=0.5$  in case 2. The x-axis represents the performance indices ( $FM$  and  $P_{available}$ ) as the objective functions, while the y-axis represents the deviations of performance.

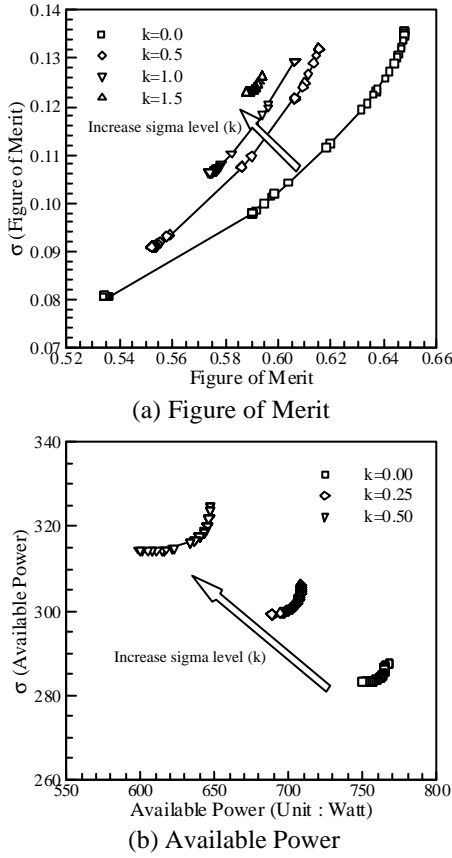


Fig. 6. Pareto optimal sets for Figure of Merit and Available Power

As shown in previous schematics, the feasible region is altered in the design space along with the increment of  $k$ . Subsequently, it results in the performance reduction with increased performance deviation, which ends up with weak robustness. On the other hand, the  $FM$  reveals that the size of the Pareto front shrinks, whereas the  $P_{available}$  has opposite characteristics along with the increment of  $k$ . In general, when the feasible region shrinks due to the  $k$  value, one expects to obtain a plot as in Fig. 6. However, when the trend of constraints is same to objective function, the plot is similar to the

Pareto front of the  $P_{available}$  plot. If  $k$  remains constant, the Pareto fronts corresponding to  $FM$  and  $P_{available}$  show the same characteristics. Because greater performance implies less robustness, or less performance implies more robustness, a trade-off is necessary between them for the best results.

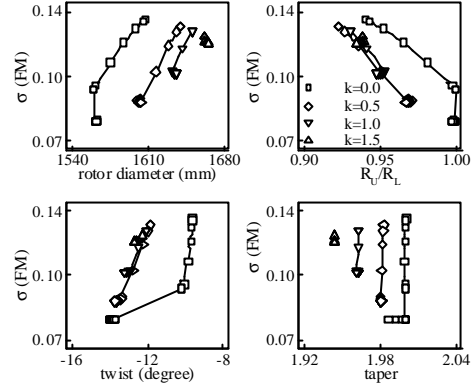


Fig. 7. Trend of design variables for robustness (Maximum Figure of Merit)

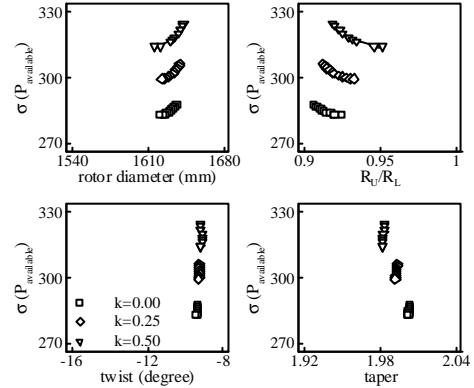


Fig. 8. Trend of design variables for robustness (Maximum Available Power)

Figs. 7 and 8 illustrate the information regarding the design variables related to the robustness (deviation) of the Pareto optima. In the case of maximizing  $FM$  (see Fig. 7), in order to assure the robustness of  $FM$  (or, to reduce the deviation of  $FM$ ) the diameter and twist tend to decrease, while the  $R_U/R_L$  increases, yet the taper is almost constant (which reveals small effectiveness of taper for the robustness of  $FM$ ). From these observations, the variables for the robustness of  $FM$  appear to contradict the physical intuition for improving  $FM$ . As a result, the design variables are determined by a trade-off between the performance and the robustness. Next, for the robustness of the constraints, the increased  $k$  results in the bigger rotor diameter

and the smaller taper. Nevertheless, the  $R_U/R_L$  and the twist turn out to have approximately the same values regardless of the value of  $k$  when taking into account the robustness ( $k \neq 0$ ).

In the case of  $P_{available}$ , as shown in Fig. 8, all plots show similar trends as the case of  $FM$  except the fact that the twist has little effect on the robustness. In contrast, three design variables (no taper variable) have almost same values with being little affected by  $k$ .

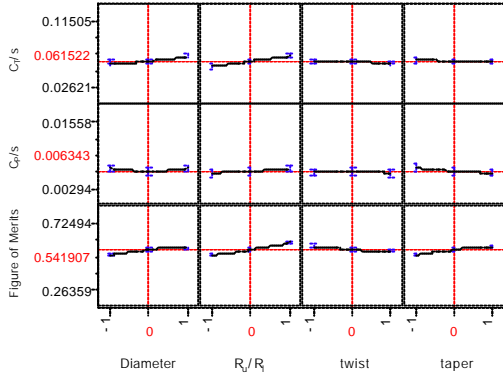


Fig. 9. Sensitivity chart of hover performance with respect to design variables

Fig. 9 represents a sensitivity chart of design variables related to the hover performance. The x-axis values -1 and 1 indicate the lower and upper bounds of each design variable which has been normalized from actual values. For instance, the twist varies from -14 to -8 degrees, thus the lower bound -1 corresponds to -14 degrees, and so on. As one can expect, the general trends shown in Fig. 9 agree with the physical intuition, namely, the  $FM$  is generally improved in conjunction with the increased rotor diameter, taper and twist angle.

In short, the trend of design variables (see Fig. 9) for improving  $FM$  and  $P_{available}$  is opposite to the trend of each (see Figs. 7 and 8). Hence, it is imperative to find a trade-off between the performance and the robustness. Unless this is the case, the higher performance indicates stronger robustness.

#### Conventional design optimization (DO) v/s robust design optimization (RDO)

Among the Pareto optimal points in Fig. 10, we choose three optima that have the following characteristic,

- The case when the performance chosen for the objective function is maximally improved ( $k=0, \delta=1$ )

- The case when the robustness for the objective function is maximally ensured ( $k=0, \delta=0$ )
- The case when the robustness for the objective function and the constraints is ensured ( $k \neq 0, \delta=0$ )

Case a) represents the results of the DO, while cases b) and c) are the results of the RDO where the minimum deviation of the objective function is found. Specifically, case b) represents when the robustness of the objective function is solely dealt with by setting the  $k$  all to zeroes in the constraints. For case c),  $k$  is randomly chosen subject to the constraints. We investigate and compare the above three cases with respect to the maximizing  $FM$  and the maximizing  $P_{available}$ .

#### Objective functions

Table 5 shows the optimized performance of the coaxial rotor UAV that maximizes  $FM$  at given constant thrust. The objective function of  $FM$  is represented in a bold typeface, and the active constraints are in an italic typeface. The sizes of the uncertainty models for the damaged area and the weight are chosen to be 5% damaged area and 0.5 kg weight increase, hence resulting in the deviation of  $FM$ . The size of uncertainty is chosen by half of the design requirements since the uncertainty varies within  $\pm 2s$  from a nominal value.

Table 5. Hover performance of the optimized coaxial rotors (max. Figure of Merit)

	Baseline	Max. Figure of Merit		
		case1-a	case1-b	case1-c
FM (deviation, s)	0.531 (0.138)	<b>0.648</b> ( <b>0.136</b> )	<b>0.535</b> ( <b>0.081</b> )	<b>0.588</b> ( <b>0.123</b> )
Thrust (N)	137.34	137.30	137.34	137.31
Autorotation index	9.286	<i>9.287</i>	<i>9.289</i>	<i>9.815</i>
Blade weight (kg)	0.552	<i>0.717</i>	<i>0.717</i>	<i>0.713</i>
Climb rate (m/min)	87.37	311.38	100.86	286.68
$P_{available}$ (W)	200.0	712.7	230.9	656.22

Fig. 10 shows the probability density function of  $FM$  corresponding to the case in Table 5, where we assumed that the performance of the baseline corresponds to a normal distribution with zero-mean and variation 1, or  $N(0,1)$ .

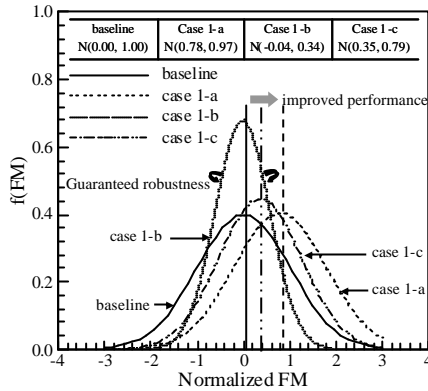


Fig. 10. Probability density function of Figure of Merit

The  $FM$  for all optimized cases show the improvement by maximally 20% (case 1-a) over the baseline design. In the case 1-b when we only focus on reducing the deviation, the performance is improved by 1%, more or less, which dictates negligible improvement. In addition, the performance in case 1-c is improved by 9% over the baseline design, which is at the same time 9% reduction from case 1-a. On the other hand, case 1-a shows a negligible deviation of  $FM$  over the baseline design, while cases 1-b and 1-c show the reduction of deviation of  $FM$  by 41% and 10%, respectively. As mentioned earlier, the reduction of the deviation means the increased robustness, hence allowing minimization of the performance degradation over uncertainty for successful mission accomplishments

For the case of maximizing  $P_{available}$  at constant thrust, Table 6 and Fig. 11 summarize the results in a similar manner in Table 5 and Fig. 10.

The  $P_{available}$  performance appears similar to the results as shown in Table 5 such that the performance decreases along the order of cases 2-a, 2-b, and 2-c. In contrast, the deviation shows different results such as 4~14% reduction from the baseline design. However, the deviations in case 2-a (without considering the robustness) and case 2-b (that takes into account the robustness of the objective function) turn out to be 2% in each case. Thus, it can be told that no performance degradation of  $P_{available}$  is improved. This is attributed to the fact that in a given design space, both the optimal point by the DO and the optimal point by the RDO are located at the same place. Meanwhile, the deviation in case 2-c is larger than that in case 2-a from the DO. As pointed out in the previous

schematics, the increase of  $k$  induces a change of the feasible region in the design space to ensure the robustness of constraints, hence resulting in excluding certain regions that have good performance and robustness. As a result, even the RDO in case 2-c yields bigger deviations over that of the DO.

Table 6. Hover performance of the optimized coaxial rotors (Maximum Available Power)

	Baseline	Max. Available Power		
		case2-a	case2-b	case2-c
FM	0.531	0.633	0.644	0.613
Thrust (N)	137.34	137.27	137.30	137.33
Autoration index	9.286	<b>9.287</b>	<b>9.288</b>	<b>9.4561</b>
Blade weight (kg)	0.552	<b>0.717</b>	<b>0.718</b>	<b>0.716</b>
Climb rate (m/min)	87.37	333.14	327.56	265.36
$P_{available}$ (W)	200.0	<b>764.86</b>	<b>749.78</b>	<b>607.41</b>
(deviation, $s$ )	(328.4)	<b>(287.0)</b>	<b>(283.2)</b>	<b>(314.2)</b>

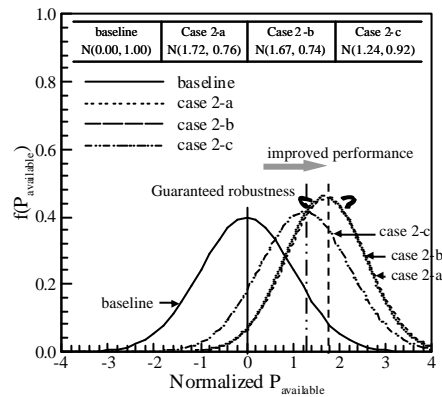


Fig. 11. Probability density function of Available Power

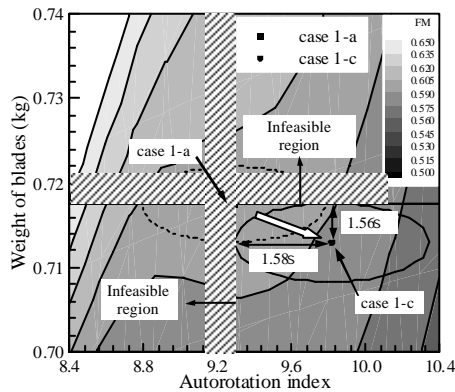
### Constraints

Table 7 summarizes the probability of violated constraints and sigma level ( $ns$ ), where active constraints are written in bold face. Both the DO (case 1-a, case 2-a) and the RDO (case 1-b and case 2-b) only for the robustness of the objective function ( $k=0$ ) have 50% of the probability of violation with respect to the constraints regarding  $AI$  and  $W_{blade}$ . The RDO taking into account the robustness of the objective function and constraints ( $k \neq 0$ ); however, this ensures the confidence level of 1.5s and 0.5s, respectively.

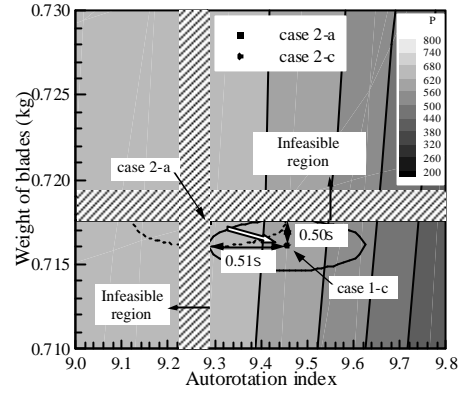
Table 7. Violation probability of constraints and the sigma level ( $ns$ )

	Max. figure of merit		
	Case 1-a	Case 1-b	Case 1-c
Autorotation index	<b>49.9%</b> (0.00s)	<b>49.7%</b> (0.01s)	5.7% (1.58s)
Blade weight (kg)	<b>48.6%</b> (0.03s)	<b>45.2%</b> (0.12s)	5.9% (1.56s)
Climb rate (m/min)	3.8% (1.78s)	<b>45.7%</b> (0.11s)	5.7% (1.58s)
Available power (W)	3.6% (1.80s)	<b>45.7%</b> (0.11s)	5.5% (1.60s)
	Max. available power		
	Case 2-a	Case 2-b	Case 2-c
Figure of Merit	25.3% (0.66s)	23.0% (0.74s)	30.0% (0.53s)
Autorotation index	<b>49.9%</b> (0.00s)	<b>49.8%</b> (0.01s)	30.5% (0.51s)
Blade weight (kg)	<b>49.0%</b> (0.03s)	<b>50.0%</b> (0.00s)	30.8% (0.50s)
Climb rate (m/min)	2.6% (1.94s)	2.9% (1.89s)	8.1% (1.40s)

The confidence levels of optimum point with respect to  $AI$  and  $W_{blade}$  constraints are shown in Fig. 12. The optimum point in case 1-a is located at the boundary of each constraints while the optimum in case 1-c is found to be relocated in the safe region, or within the feasible region. The confidence intervals corresponding to each optimum point are drawn by ellipses, which represent the regions where the performance variations are allowed. Thus, the  $AI$  in the case 1-c corresponds to the probability of achieving the target value by 5.7% upon the ballistic damage of 10% of the blade area.



(a) Maximum *Figure of Merit*



(b) Maximum *Available Power*

Fig. 12. Active constraints & confidence intervals

As shown in the figures, each confidence interval does not overlap with the infeasible region but stays in the feasible region. Hence, it is possible to conclude that RDO ensures the robustness of constraints. This fact claims several meaningful results that the optimized coaxial rotor is likely to achieve a safe landing under emergency situation, as well as the reduction of the required power from decreasing the  $W_{blade}$ . In other words, the optimized coaxial rotor designed by RDO is likely to meet the safety criterion, while accomplishing the missions successfully.

### Design Variables

The geometric parameters of the optimized coaxial rotor configurations are shown in Table 8. The increase in the rotor diameter induces several disadvantages such as the overall dimension, cost, weight, and the torque limit of the gear box. The main concern is to determine the smallest rotor diameter which guarantees a safe landing. The reason why rotor diameter does not hit the upper bound is attributed by incorporating the  $AI$ . In addition, excessive taper may cause the low Reynolds number effect around the tip region, thus leading to structural instability. In order to prevent the blade from ending up with an overly slender tip, the  $W_{blade}$  constraint is imposed such that the taper ratio does not exceed 2, as given in Table 8. By employing the maximum taper ratio of 2, it could be possibly expected that the 5-6% decrease in the induced power by tapering the outer 50% of the blade span with a factor of two.[11]

Table 8. Geometry of the optimized coaxial rotors

		Rotor diameter (mm)	$R_U/R_L$	Twist (degree)	Taper
baseline		1572.00	1.00	0.00	1.00
Max. FM	case1-a	1608.17	0.94	-9.64	2.00
	case1-b	1562.27	1.00	-13.84	2.00
	case1-c	1666.72	0.93	-12.74	1.94
Max. $P_{available}$	case2-a	1635.33	0.91	-9.36	2.00
	case2-b	1621.55	0.92	-9.44	2.00
	case2-c	1619.09	0.95	-9.15	1.98

Andrew [17] and Leishman [3] discussed the possibility of improving coaxial rotor performance through the use of different sizes of the upper and the lower rotors. It follows from the analytical model that decreasing the upper rotor radius by 8% could improve hover performance, which is due to the fact that the lower rotor disc takes undisturbed air over a larger portion instead of disturbed air downstream after the upper rotor disc. The results of  $R_U/R_L$  in Table 8 are consistent with the discussion given by Andrew and Leishman.

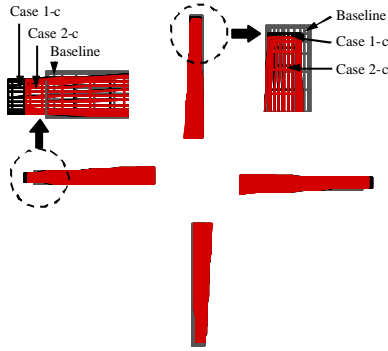


Fig. 13. Optimized coaxial rotor configurations (baseline, case 1-c and case 2-c)

In order to ensure the robustness of the objective function in the RDO as compared to the DO (case 1-a, case 2-a), the rotor diameter should be reduced (case 1-b, case 2-b). In contrast, the rotor diameter should be increased for the robustness of the  $AI$  constraint. (case 1-c, case 2-c) From this trade-off relationship, case 1-c and case 2-c are ascertained to yield the proper diameter along with appropriate choice of the sigma level. Also, because the taper in the problem of maximizing  $FM$  or  $P_{available}$  must be determined along with the variation of  $k$  value, which ends up with slight decrease to assure the

robustness of the  $W_{blade}$  constraint. The results of  $R_U/R_L$  and twist are shown such that the design is done not to ensure the robustness but to improve the rotor performance. The coaxial rotors for UAV proposed from this research are case 1-c and case 2-c as shown in Fig. 13.

## Conclusions

Robust design optimization for coaxial rotor is performed to maximize the performance and to minimize the performance degradation caused by uncertainties such as ballistic damage of rotor blade, weight variation due to mission change, and toleration of the geometry. Multi-objective functions consist of rotor performance and its deviation by incorporating four design variables of rotor diameter, differential rotor ratio, twist, and taper, which are to be optimized for robust rotor blade under uncertainties. From these results, we can conclude with the following statements.

First of all, we manage to perform a coaxial rotor design that satisfies the design requirements by employing either a DO or the RDO. By the conventional design, the probability to accomplish the missions in success under uncertainties such as ballistic damage or weight variation goes up as low as 50%, however, the probability can be improved by 70~95% by employing the robust design method. Consequently, even with 10% blade damage and 1kg of weight increase the optimized coaxial rotor UAV from RDO is most likely to accomplish missions in success.

Second, the Pareto optimal set is obtained by modifying weights of the multi-objective function, and subsequently a trade-off relationship between two optimization cases for figure of merit and available power is confirmed. The robustness is ensured by reduced performance deviation in conjunction with smaller rotor diameter and larger differential rotor radii, resulting in minimum performance degradation. Small twist ensures the robustness of figure of merit, yet a contrary effect on available power. The taper has no effect on the robustness of figure of merit and available power. This tendency contradicts the anticipated tendency of design variables to improve performance.

Finally, we encounter the cases where the feasible region in the design space is altered in conjunction with the increase of the sigma level to ensure the robustness of constraints. This results in a modification of the region that contains not only good performance design but

also strong robust design. In particular, in the case of the available power, the optimum point obtained from a conventional design matches with the robust optimum; thus, both the performance and the robustness are diminished when the sigma level changes.

### Acknowledgement

This study has been supported by the KARI under KHP Dual-Use Component Development Program funded by the MKE and the second stage of the Brain Korea 21 Project in 2008.

### References

1. J.G. Leishman, S. Ananthan, Aerodynamic Optimization of a Coaxial Proprotor, 62<sup>nd</sup> Annual Forum and Technology Display of the American Helicopter Society, Phoenix, May 9-11, 2006
2. Y. Byun, J. Lee, K. Yee, T. Gu, W. Song and B. Kang, Re-design of the Coaxial UAV's Platform for an Improvement in Performance, Proceeding of the 2007 KSAS Fall Conference, KSAS07-2204, 2007
3. J.G. Leishman, Principles of Helicopter Aerodynamics, second ed., Cambridge University Press, Cambridge, 2006
4. G Taguchi, Taguchi on Robust Technology Development, ASME Press, New York, 1993.
5. D.A. DeLaurentis and D.N. Mavris, Uncertainty Modeling and Management in Multidisciplinary Analysis and Synthesis, Proceedings of 38th AIAA Aerospace Science Meeting and Exhibit, 2000
6. X. Du and W. Chen, Efficient Uncertainty Analysis Methods for Multidisciplinary Robust Design, AIAA Journal, 2002, 40 (3) pp. 545-552
7. B.D. Youn, K.K. Choi and Y.H. Park, Hybrid Analysis Method for Reliability-Based Design Optimization, Journal of Mechanical Design, 2003, 125 (2) pp. 221-232
8. M.M. Putko, P.A. Newman, A.C. Taylor III and L.L. Green, Approach for Uncertainty Propagation and Robust Design in CFD Using Sensitivity Derivatives, Journal of Fluids Engineering, 2002, 124 (1) pp. 60-69
9. S. Jun, Y.H. Jeon, J. Rho, J.H. Kim, J. Kim and D.H. Lee, Reliability-Based and Robust Design Optimization with Artificial Neural Network, 6th World Congresses of Structural and Multidisciplinary Optimization, 2005
10. A. Papoulis and S.U. Pillai, Probability, Random Variables and Stochastic Processes, Fourth edition, McGraw-Hill, New York, USA, 2002
11. D.A. Wachspress and T.R. Quackenbush, Impact of Rotor Design on Coaxial Rotor Performance, Wake Geometry and Noise, The American Helicopter Society 62<sup>nd</sup> Annual Forum, Phoenix, May 9-11, 2006
12. J. Lee, K. Yee and S. Oh, Parametric Study of Coaxial Rotor Performance in Hover, Aerospace Science and Technology, 2008, submitted
13. J.G. Leishman, Experimental Investigation into the Aerodynamic Characteristics of Helicopter Rotor Airfoils with Ballistic Damage, United States Army Research Laboratory, Report ARL-CR-295, 1996
14. M.G. Potapczuk and J.J. Reinmann, Icing Simulation: A Survey of Computer Models and Experimental Facilities, AGARD CP-496, 5.1-5.27., 1991
15. H. Kim, M.B. Bragg, "Effects of Leading-Edge ice Accretion Geometry on Airfoil Aerodynamics," AIAA Paper 99-3150, 1999.
16. J.A. Freeman and D.M. Skapura, Neural Networks Algorithm, Applications, and Programming Techniques, Addison-Wesley Publishing Company, 1992
17. M.J. Andrew, Coaxial Rotor Aerodynamics in Hover, Vertica, Vol. 5, 1981